High-precision U—Pb zircon dating of explosive volcanism in an early bi-modal volcano-sedimentary sequence from the Isle of Mull, North Atlantic Igneous Province

J.M. Millett [a,b,*], D.W. Jolley [b], M.J. Hole [b], L. Augland [c], J.H. Pugsley [b], G.W. McLeod [d], S. Planke [a,c]

[a] *Volcanic Basin Energy Research AS, Oslo, Norway*
[b] *Department of Geology and Geophysics, University of Aberdeen, UK*
[c] *Department of Geosciences, University of Oslo, Oslo, Norway*
[d] *School of Earth and Environment, University of Leeds, UK*

A B S T R A C T

The North Atlantic Igneous Province (NAIP) forms one of the best studied Large Igneous Provinces (LIP) on the planet, however, significant uncertainties regarding the age and nature of the early onset of volcanism across the province remain. In order to better understand the onset and timing of volcanism within the NAIP, we present a new study of the mixed volcano-sedimentary deposits exposed at the base of the Isle of Mull lava pile, Inner Hebrides, Scotland. The study area comprises organic rich estuarine sediments, intimately mixed and interdigitated with bi-modal composition volcaniclastic and pyroclastic interlayers, including a prominent stratigraphically constrained c. 30 cm thick water-lain rhyolitic ignimbrite. Pristine magmatic zircons liberated from the ignimbrite reveal a high precision U—Pb age of 62.035 ± 0.041 Ma (2σ) giving a robust age for early volcanism in this part of the province. Field observations reveal evidence for mafic phreatomagmatic eruptive deposits both above and below the rhyolite documenting the bimodal explosive nature of the initial magmatism in this area and, importantly, that mafic magmatism initiated before the dated unit. The bi-modal explosive eruptions periodically inundated an otherwise quiet and low energy Danian aged estuarine environment prior to its inundation with lava as magmatism took hold in the region.

1. Introduction

The North Atlantic Igneous Province (NAIP) comprises one of the most extensive Large Igneous Provinces (LIPs) on Earth covering an estimated area of c. 1.3×10^6 km² (Eldholm and Grue, 1994; Saunders et al., 1997). NAIP volcanism is believed to have initiated as early as 64 Ma within the mid-Danian stage of the Palaeocene and to have continued sporadically for several million years until large scale volcanism associated with rifting led to continental break-up in the Early Eocene at around 54 Ma (Wilkinson et al., 2017). Within this c. 10 Myr period, the North Atlantic region underwent a complex geological history involving changes in relative plate motions (Jones et al., 2017), seafloor spreading in the Labrador Sea and Baffin Bay area (Abdelmalak et al., 2019), cessation of Alpine compression between Africa and Europe (Nielsen et al., 2007), mantle temperature fluctuations (Millett

et al., 2020), globally warm but fluctuating climate peaking in the PETM (Palaeocene-Eocene Thermal Maximum) hyperthermal at c. 56 Ma (Berndt et al., 2023), alongside major environmental and ecosystem changes associated with volcanism within changing eruption environments (Jolley et al., 2012, 2021, 2024, Millett et al., 2021). Understanding the linkages and potential feedbacks between NAIP magmatism and these temporally associated events continues to receive intense study and debate (Berndt et al., 2023; Hole and Natland, 2020; Nielsen et al., 2007; Schiffer et al., 2020; Svensen et al., 2004).

Robust age constraints are critical for appraising the evolution of the NAIP. A large number of age determinations have been published utilizing Ar/Ar, K/Ar, Rb/Sr and Re/Os methods, however, generally low precision ($> \pm 0.4$ Ma 2σ error) and quality control issues restrict their utilization for understanding the detailed temporal evolution of the province (Wilkinson et al., 2017). Across the province, significant

uncertainty remains for large geographical areas where very few if any samples have been retrieved, especially in the offshore areas such as Hatton Bank, Rockall Basin and large parts of the northern Faroe-Shetland, Møre, and Vøring basins (Jolley et al., 2021; Planke et al., 2023). However, this uncertainty also prevails within many well studied onshore areas (Wilkinson et al., 2017). The fundamental challenge for dating the NAIP is that the majority of the magmatic rocks by volume comprise low-K basaltic rocks which do not contain minerals suitable for high precision methods such as U—Pb, and often present challenges for deriving robust and repeatable $^{40}Ar/^{39}Ar$ dating results (Kelley, 2002; Wilkinson et al., 2017), a problem that has also been encountered in other basalt dominated provinces (Baksi et al., 2013).

Biostratigraphical studies of sedimentary strata within the basins surrounding the NAIP and from inter-lava sediments provide important environmental and relative timescale indicators for the ecosystem response of the Palaeogene climate to NAIP volcanism (Jolley et al., 2012; Jolley et al., 2021). However, for much of the NAIP volcanic sequences including almost all of the occurrences of sedimentary interbeds outcropping onshore, terrestrial dominated assemblages often lack unequivocally age diagnostic flora or marine dinocyst assemblages. This has restricted the potential for direct on to offshore correlations and has led to conflicting interpretations of province age evolution (Jolley et al., 2002, 2021, 2024; Stoker et al., 2018; Storey et al., 2007).

The U—Pb method has been successfully applied in a small number of cases where suitable minerals such as zircon have been identified and analysed in the NAIP. In the Hebrides of Scotland, Hamilton et al. (1998) reported air abraded (AA) ID-TIMS U—Pb zircon ages of 60.53 ± 0.08 Ma and 58.9 ± 0.06 Ma for the Rum and Skye central complexes respectively (both to 2σ), however, these ages represent intrusive events. In terms of stratigraphically constrained dates, an AA ID-TIMS U—Pb zircon age of 61.15 ± 0.25 Ma (2σ) was presented for the Muck Tuff (Chambers et al., 2005) whilst the Tardree rhyolite from Ireland is dated by CA-ID-TIMS as 61.32 ± 0.09 Ma (2σ) making it to our knowledge the oldest high precision age within the NAIP to date (Ganerød et al., 2011). Drake et al. (2022) recently published a new CA-ID-TIMS U—Pb age of 56.15 ± 0.10 Ma (2σ) from zircons collected from within Stage 3 of the Kilchrist Volcanic Formation on Skye. Older high precision U—Pb ages possibly related to NAIP magmatism exist for distal ash layers identified far to the north of the NAIP, such as a weighted mean CA-ID-TIMS 61.596 ± 0.028 Ma (2σ) age from Svalbard (Jones et al., 2017). Clearly, new high precision isotopic age dates from the volcanic sequences are critical for improving the understanding of temporal links between magmatism, environment, and climate during the Palaeogene (Berndt et al., 2023; Jones et al., 2017; Svensen et al., 2004).

In this contribution, we investigate some of the lowermost exposed volcanic deposits on the Isle of Mull, one of the major igneous centres and associated lava fields of the NAIP (Emeleus et al., 2005). This study focuses on the Carraig Mhór locality outcropping on the south coast of the island where the sequence comprises spectacular examples of the intimate interaction between punctuated effusive and explosive volcanism and a pre-existing graben-constrained sedimentary drainage system, previously referred to as the 'Staffa Formation' (Brown and Bell, 2007; Jolley et al., 2009; Williamson and Bell, 2012), although its definition as a formal formation is challenging (Jolley et al., 2024). Within this sequence numerous graded volcaniclastic beds are interdigitated and mixed with organic rich quartz bearing sediments alongside a complex array of volcanic lithologies and minor intrusions documented by Brown (2003), and Brown and Bell (2007) including a well-preserved rhyolitic ignimbrite layer here named the Carraig Mhór Ignimbrite.

The complexity of the Carraig Mhór locality and the presence of a zircon bearing stratigraphically constrained ignimbrite merits further analyses both in terms of the volcanological and environmental evolution of the early NAIP but also as a candidate for high precision U—Pb dating (Brown, 2003). Within this study, we present a reappraisal of the volcano-sedimentary evolution of the Carraig Mhór graben sequence building on and testing hypothesis put forward previously, alongside presenting a new high precision age date for this part of the province.

Field evidence is presented in support of basaltic phreatomagmatic explosive eruptions generated through interaction of the Carraig Mhór magmatic system with pre- and syn-volcanic sedimentary systems. We propose that these and associated processes can explain much of the textural and bedding features found within the main Carraig Mhór volcano-sedimentary successions reducing the requirement for intrusive processes to the clear cross-cutting minor intrusions with locally peperitized margins. Pristine magmatic zircons, liberated from the Carraig Mhór Ignimbrite were analysed by U—Pb chemical abrasion - isotope dilution - thermal ionisation mass spectrometry (CA-ID-TIMS) and give a mean weighted age of 62.035 ± 0.041 Ma (2σ). These results, to our knowledge, reveal the oldest high-precision stratigraphically constrained age determination for the NAIP, pushing back the onset of magmatism at this location (Wilkinson et al., 2017). One of the most intriguing observations of the studied section is that multiple normally graded volcaniclastic layers, many including basaltic fragments, are identified both above and below the Carraig Mhór Ignimbrite. These layers are clearly separate from local examples of peperite formation at intrusion margins (Brown and Bell, 2007), and form thin continuous stratigraphic layers. By inference, basaltic volcanism was already ongoing in the area prior to the dated Carraig Mhór Ignimbrite eruption. This study provides important new constraints on the age and nature of early NAIP bi-modal volcanism and highlights the potential for further dating efforts in this unique example of an onshore Danian sedimentary sequence in the heart of the British Palaeogene Igneous Province.

2. Methods

Field investigations at the Carraig Mhór locality on Mull were undertaken to characterize and map the volcanic and associated sedimentary sequences which occur below and inter-layered with the Staffa Type chemistry lava flows (Brown and Bell, 2007; Jolley et al., 2009, 2024; Williamson and Bell, 2012). Samples were collected for both petrographic and palynological analyses from key sedimentary units focusing on the lowermost sequence accessible during low spring tide. A single large sample (c. 2 kg) was collected for age dating from the prominent strata-bound ignimbrite unit on the foreshore.

2.1. Petrography and SEM

In total, 8 polished and uncovered thin sections were made from the foreshore volcaniclastic and ignimbrite bearing sequence. Thin sections were analysed by scanning electron microscope (SEM) at the University of Aberdeen with a high-resolution Carl Zeiss Gemini SEM 300 which is a field emission gun (FEGSEM) high resolution SEM. The analytical system is supplied by Oxford Instruments and consists of an AZtec Energy EDS analysis system with an XMax 80 detector and an AZtecHKL EBSD analysis system with a Nordlys Nano EBSD camera. Oxford Instruments AZtec Energy and AZtec HKL software suites were used for analysis.

2.2. Geochemistry

A single sample of the Carraig Mhór Ignimbrite was analysed by ICP-MS and ICP-OES by Chemostrat in order to compare to existing geochemistry from the Carraig Mhór sequence (Jolley et al., 2024). The sample was crushed in agate and analysed using a standard laboratory approach including analysing blanks and international reference standards to monitor for precision and accuracy. The geochemical analyses of the Carraig Mhór Ignimbrite is presented in the online supplementary data A1.

2.3. Palynology

32 samples were taken for palynological analysis from sedimentary units in field sections. These were processed following standard techniques, including HF digestion, boiling in 37% HCl to remove precipitates and oxidation for 5 min in dilute 70% Nitric acid where necessary. Coal samples were prepared by dissolution using fuming nitric acid. The resultant >7 μm residues were mounted in a permanent petropoxy mounting medium and examined under a transmitted light Olympus BX53 microscope. For each sample, counts of 250 specimens were targeted, but with the highly variable recovery from inter lava field sedimentary rocks, frequently not attained. Accordingly, data was normalized as square roots.

2.4. U—Pb isotopic age dating

Sample LEA17–1 from the Carraig Mhór Ignimbrite was crushed, pulverised and reduced on a Wilfley table before heavy minerals were separated through standard magnetic and heavy liquid techniques at the University of Oslo. The zircons were imaged by cathodoluminescence (CL)-SEM and subsequently selected under an optical microscope, annealed for c. 72 h at c. 900 °C and chemically abraded with HF (+HNO$_3$) at c. 195 °C for 14 h (Huyskens et al., 2016; Mattinson, 2005). The zircons grains chosen for analyses were spiked with a mixed ^{202}Pb-^{205}Pb-^{235}U tracer that has been calibrated to the EARTHTIME (ET) 100 Ma solution (Ballo et al., 2019), which allows direct comparison of dates generated with our in-house tracer with dates generated by the ET tracers (assuring that tracer calibration uncertainties are included in the ages when compared). After spiking, the zircons were dissolved in HF (+HNO$_3$) at c. 210 °C for >48 h in Teflon micro capsules enclosed in a Parr type Teflon bomb. The solutions were subsequently chemically separated through column chemistry (separating U and Pb from REE's and other ionisation inhibiting elements). The solutions were loaded on zone refined Re filaments and measured on a Finnigan MAT262 TIMS.

For all samples Pb was measured in dynamic mode on a Masscom secondary electron multiplier and U in static mode on Faraday cups. Corrections for Pb fractionation were made using the measured ^{202}Pb/^{205}Pb-ratios for each Pb analysis relative to the ^{202}Pb/^{205}Pb-ratio of the tracer of 2.2702 (±0.006%, 2σ). The long-time average U-fractionation determined from measurements of the U500 standard solution (0.07%/a.m.u. ±0.04%, 2σ) was used to correct for sample U-fractionation. Pb blanks are generally <1 pg. The raw data were reduced using Tripoli (Bowring et al., 2011) and analytical errors and corrections (including tracer uncertainties and Th-corrections, assuming Th/U in the magma of 3) were incorporated and propagated, and dates calculated using an Excel macro based on published algorithms (Schmitz and Schoene, 2007) with specified decay constants (Jaffey et al., 1971). Data were visualised using ISOPLOT (Ludwig, 2003) and dates and the presented weighted mean age are reported with uncertainties as ±x/y/z, where x is the analytical uncertainty, y represent analytical and tracer calibration uncertainties combined, and z represent the analytical uncertainty, tracer calibration uncertainty and the decay constant uncertainties combined. The U—Pb analyses of the Carraig Mhór Ignimbrite zircons are presented in the online supplementary data A2.

2.5. Lu—Hf isotope analysis

Nine zircons from the LEA17–1 sample were analysed for Lu—Hf isotopes by solution inductively coupled plasma mass spectrometry (S-ICPMS) at the Department of Geosciences, University of Oslo following the routine of Augland and David (2015), modified from Patchett and Tatsumoto (1981) and Augland et al. (2012). Washes from the chemical separation of U and Pb of dissolved zircons were converted to a 1 N HCl–0.1 N HF solution and an aliquot was taken for the determination of Lu/Hf-ratios. The remaining solutions were run through a one-stage cation exchange column chemistry for Hf-purification. We measured

Hf isotopes on a NU Plasma HR multi-collector ICP-MS fitted with a NU instruments DSN-100 desolvating nebulizer. Measurement procedures and data reduction routines followed those described in Augland and David (2015). The ^{176}Lu/^{177}Hf-ratios were measured on the untreated aliquots with a Bruker Aurora M90 single collector ICP-MS following the procedure of Augland and David (2015). Measured Lu/Hf-ratios were corrected for isobaric interferences of Lu and Hf based on measured ^{172}Yb and ^{175}Lu and the measured and the corrected ^{175}Lu/^{177}Hf was used to calculate the ^{176}Lu/^{177}Hf ratios reported in the online supplementary data A3, based on the terrestrial average ^{176}Lu/ ^{175}Lu of 0.02656 (Blichert-Toft and Albarède, 1997). A value of 1.867×10^{-11} a^{-1} for the decay constant of ^{176}Lu was used in all calculations (Scherer et al., 2001; Söderlund et al., 2004). For the calculations of ε$_{Hf}$ we use present-day chondritic ^{176}Hf/^{177}Hf = 0.282785 and ^{176}Lu/^{177}Hf = 0.0336 (Bouvier et al., 2008). Reference solution JMC-475 (courtesy of Jonathan Patchett, The University of Arizona) was run at frequent intervals obtaining ^{176}Hf/^{177}Hf = 0.282180 ± 0.000022 (2σ; 6 analyses), overlapping the generally accepted value of 0.282161 ± 0.000014 (Blichert-Toft and Albarède, 1997). The external 2σ precision is thus considered to be 0.008%, and when internal precision of the average values is lower than this, a 2σ of 0.008% was used in calculation of initial ^{176}Hf/^{177}Hf (^{176}Hf/^{177}Hf$_{(t)}$) and initial ε$_{Hf}$ (ε$_{Hf(t)}$). The data presented in the online supplementary data A3 are normalized to the accepted value of JMC-475 (Blichert-Toft and Albarède, 1997) and errors have been propagated using the algorithms of Ickert (2013). The reported ε$_{Hf(t)}$ and ^{176}Hf/^{177}Hf$_{(t)}$ values are calculated at the interpreted U—Pb age of the rock.

3. Geological setting

The Palaeogene volcanic successions of the Isle of Mull, NW Scotland, have been studied in detail for well over a century (Duke, 1851; Gardner, 1887) and have been integral in shaping the development and understanding of modern petrogenesis and volcanology (e.g. Bailey, 1924; Emeleus et al., 2005). The extrusive volcanic succession on Mull is dominated by c. 1800 m of stepped erosional remnants of plateau lavas. Three main lava series make up the majority of the Mull volcanic pile including the mildly alkaline Mull Plateau Lava Formation (MPLF), the Coire Gorm (CG) magma type, and, the Central Mull Tholeiites (CMT), (Kerr et al., 1999). Towards the base of the lava pile significant stratigraphic geochemical variations occur including the highly crustal contaminated 'Staffa' magma type which have been compared with sedimentary interbed ecosystem developments to reappraise the early development of the Mull lava pile (Jolley et al., 2024).

The basal contact of the volcanic successions on Mull are best exposed at Carsaig Bay and on the northern Ardmeanach peninsula (Fig. 1). These localities display the contact between younger Plateau lavas and palaeo-highs of Mesozoic to basement rocks (Jolley et al., 2024; Williamson and Bell, 2012). The earliest exposed examples of volcanic deposits on Mull can be studied within two prominent NNW-SSE trending graben constrained palaeo-valleys located in SW modern day Mull (Fig. 1). Within the graben-fill numerous sedimentary interlayers (Gardner, 1887; Jolley et al., 2009, 2024) and stunningly columnar ponded lavas (Bailey, 1924; Jolley et al., 2024; Williamson and Bell, 2012) accumulated in constrained accommodation.

The Carraig Mhór section, the focus of this study, only receives passing mention in the Mull Memoir in reference to Area 1, Sheet 44, where the main Carraig Mhór Bed (later defined by Brown and Bell, 2007) is described by B. Lightfoot (Bailey, 1924). Brown and Bell (2007) present a detailed study of the sequence focusing on the Carraig Mhór Bed (CMB), which occurs as a prominent inter-layer between some of the earliest lava flows of the Mull sequence at this locality. Famelli et al. (2021) presented new field evidence from the Carraig Mhór locality supporting an effusive rather than intrusive origin for the lower-most lava unit including evidence for deposits associated with rootless cone development. This was followed by Jolley et al. (2024) who presented
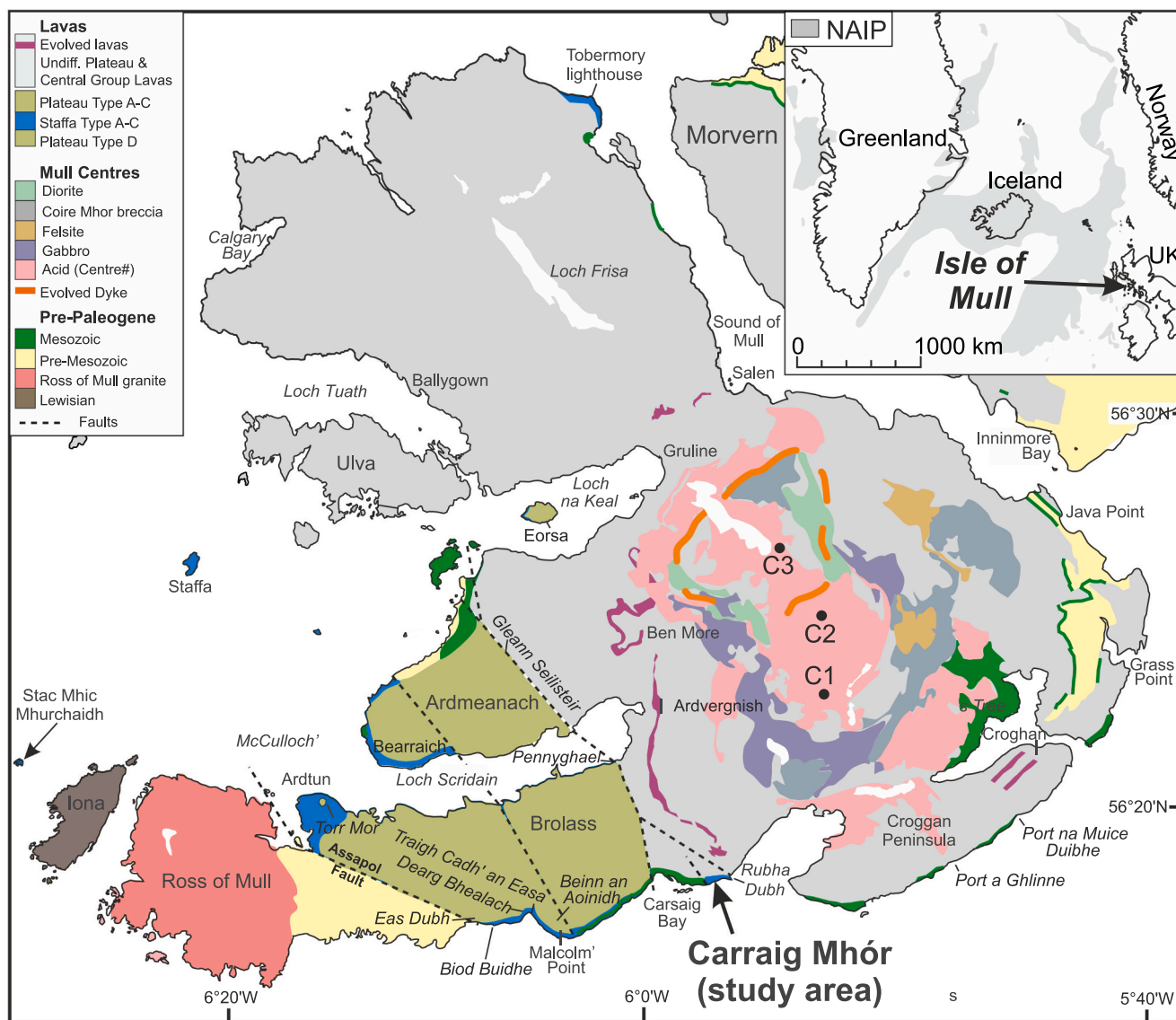
Fig. 1. Map of Mull showing the location of the Carraig Mhór study area modified after Bailey (1924) and Jolley et al. (2024), with inset simplified distribution map of the wider NAIP after Horni et al. (2017).

new palynological evidence supporting a potentially lower temperature emplacement of the Carraig Mhór Bed. The sequence at Carraig Mhór reveals significant complexity with highly varied and intricate relationships between sedimentary, pyroclastic, effusive and intrusive processes.

4. Results

4.1. Geology of the Carraig Mhór graben sequence

Fig. 2a presents a schematic cross section through the Carraig Mhór sequence (see Jolley et al., 2024 for a photogrammetry model of the exposures). The development of the exposed graben fill at Carraig Mhór (at low spring tide) to the top of the lower cliff can be broadly separated into six main phases based on a separation of in-situ effusive basaltic lava flows (L1, L2, and L3) each overlying sedimentary / volcaniclastic dominated units. The main intervals correspond to the revised stratigraphy of Jolley et al. (2024) as follows:

L3: Effusive lava (Staffa Type C chemistry)
CMB: The Carraig Mhór Bed (Brown and Bell, 2007)
L2: Effusive lava (Staffa Type C chemistry)

AIU: Ardtun Interbed (Upper)
L1: Effusive lava (Staffa Type A chemistry)
AIL: Ardtun Interbed (Lower)

Detailed descriptions of the effusive intervals are available in the literature (Brown and Bell, 2007; Famelli et al., 2021; Jolley et al., 2024; Williamson and Bell, 2012) and will not be repeated here other than in relation to their contacts and interactions with the sediment dominated intervals. The lowermost AIL comprises a sequence dominated by numerous often normally graded thin, typically 5–20 cm, beds of mixed siliciclastic and volcaniclastic material (Figs. 2 and 3c). The volcaniclastic components of the sediments range from >90% down to locally <10% in more siliciclastic dominated shaley and sandstone layers (Fig. 2b). Clast percentage-based sub-division and classification (e.g. Fisher and Schmincke, 2012) of the finely bedded AIL sediments, which show rapid fluctuations in proportions of pyroclastic, epiclastic, and siliciclastic (rounded quartz grains) components is not attempted within this study, and instead the general term 'volcaniclastic' is used to describe the general sequence. We justify this in relation to the focus of this paper, and by the rapid fluctuations of clast proportions across arbitrary percentage (e.g. 75% pyroclastic components) classification boundaries throughout the sequence, in several cases occurring within
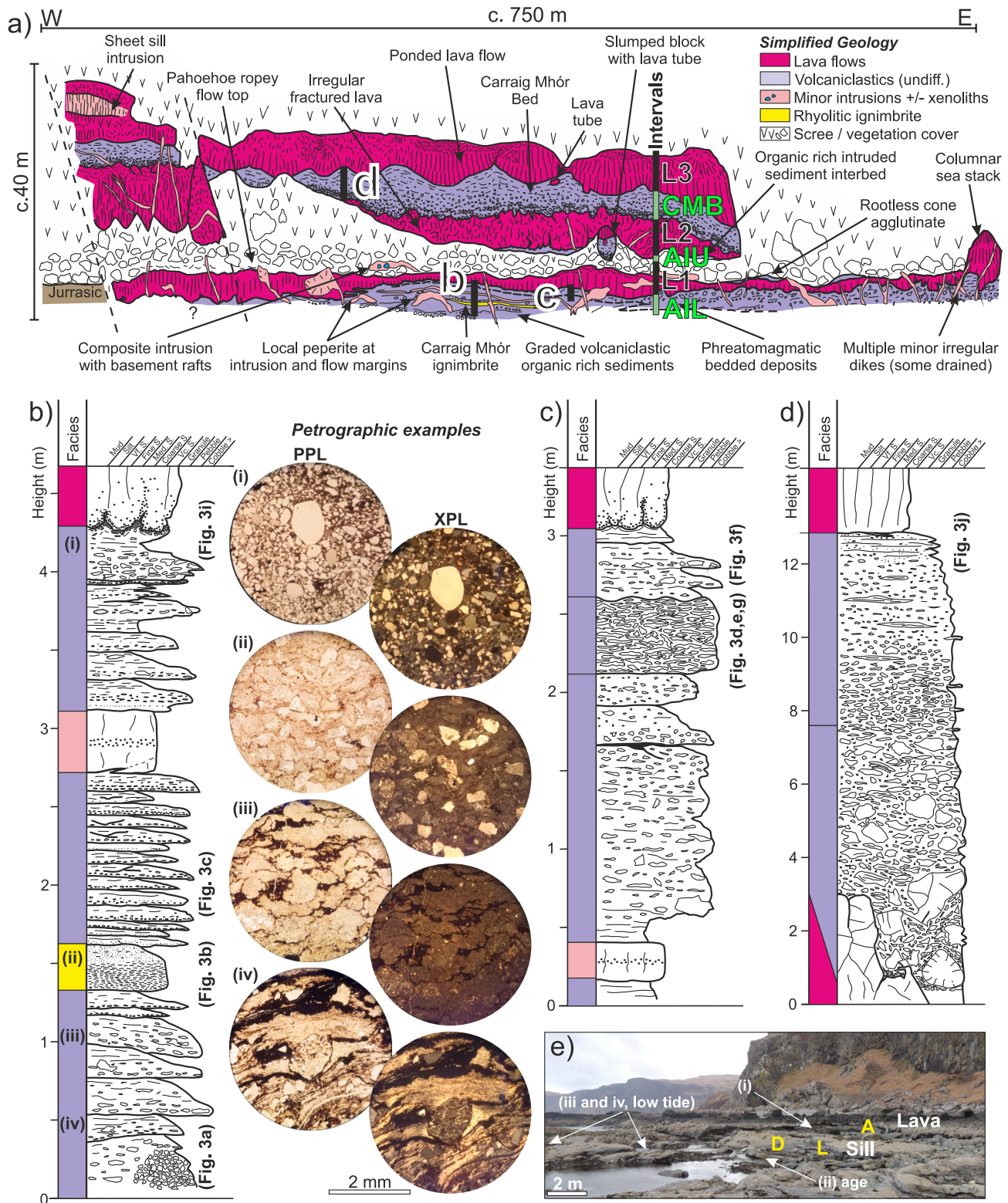
Fig. 2. a) Schematic cross-section of the Carraig Mhór locality showing the relationship between the main effusive and sedimentary sequences. The sequence is divided into three main sediment dominated intervals after Jolley et al. (2024) including AIL: Ardtun Interbed (Lower); AIU: Ardtun Interbed (Upper); CMB: Carraig Mhór Bed), each overlain by effusive lava flows named sequentially in stratigraphic order: L1, L2, and L3. b) Composite graphic facies log through the main fore-shore sedimentary dominated sequence of the AIL. Petrographic examples of textures within the sequence are shown in plain polarized light (ppl), and cross polarized (XPL) light for context. c) Graphic facies log highlighting lateral facies variations within the uppermost AIL including basaltic phreatomagmatic pyroclastic deposits. d) Composite graphic facies log through the main Carraig Mhór Bed highlighting the sharp irregular and smooth lower and upper lava contacts respectively. e) Field picture looking west from the c) log locality showing key features of the foreshore AIL sequence. D: dinoflagellate cyst *Operculodinium* spp.; L: mat containing broad leaf fossils; A: common green algae (*Pediastrum bifidites*). (For interpretation of the references to colour in this figure legend, the reader is referred to the web version of this article.)
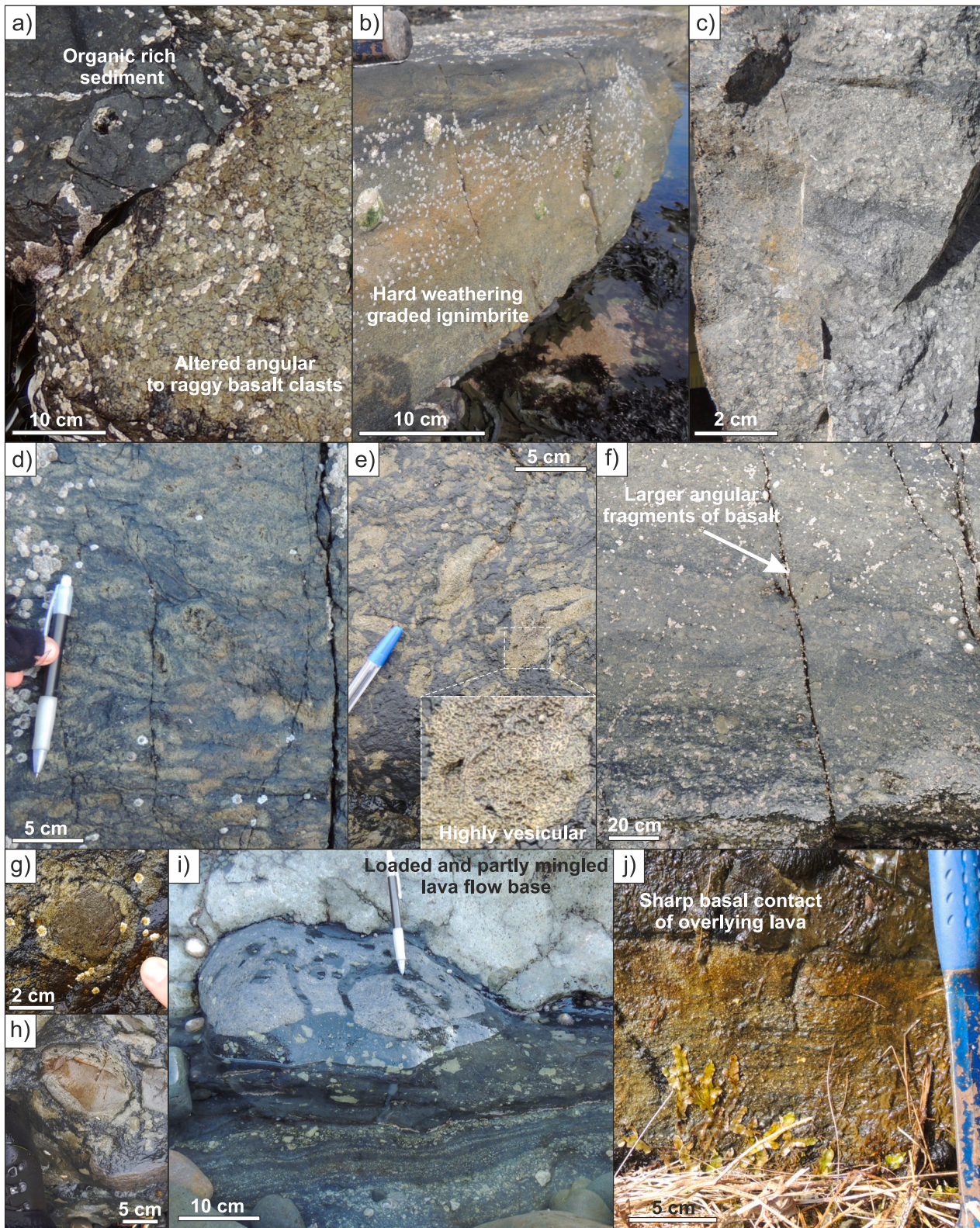
Fig. 3. Field outcrop examples from the Carraig Mhór graben sequence, locations marked in Fig. 2. a) Pod-like body of basaltic close-packed angular to raggy clasts within organic rich sediments. b) Hard weathering normally graded Carraig Mhór Ignimbrite. c) Thin beds of fining up graded volcaniclastic layers mixed with organic rich quartz bearing sediments. d) Raggy basaltic spatter-like pyroclasts with prominent bedding parallel elongation and plastic deformation mixed with organic rich sediments. e) Raggy pyroclasts highlighting highly vesicular nature of spatter-like textures mixed with sediment. f) Layered phreatomagmatic deposits with stringers of mixed organic rich sediments within prominent wedge thinning out to the west across the Carraig Mhór fore-shore. g) Example of bomb cored with non-vesicular basalt fragment from the Ardtun Interbed (Upper). h) Example of bomb cored with non-vesicular basalt fragment in foreshore boulder. i) Basalt lava contact with AIL highlighting local mingling and loading of clearly bedded organic rich volcaniclastic layers. j) Sharp basal contact of basalt lava with the top of the CMB bedded volcaniclastic sediments.

individual beds.

In Fig. 2b an annotated composite log through AIL from the base of a near-continuously exposed section is presented. The lowest exposed stratigraphic deposits are poorly exposed and comprise a mixture of variably bedded to massive organic rich sediments with variable components of mixed basaltic clasts (Fig. 2b). In one example an irregular pod-like body composed of close packed fluidal to angular altered basaltic clasts is observed (Fig. 3a) invoking post-depositional fluidization and possible injection. The volcanic clasts display mixed morphologies ranging from angular basaltic crystalline blocky to scoriaceous clasts, through to raggy and plastically deformed pyroclastic morphologies including spatter and fiamme-like structures (Figs. 2b and 3a). The pyroclasts have been replaced by secondary alteration minerals and in several cases comprise the dominant clast type of thin beds. Petrographic and SEM backscatter data reveals plastically distorted pyroclasts which are seen to wrap around rotated crystalline basalt clasts in some cases giving welding textures (Figs. 2b and 4). Composition of the microcrystalline mosaics (alteration replacement) that make up the pyroclasts fluctuates from more Mg rich to more Si rich implying that mixed composition melts formed the parent magmas for these deposits although variable degrees of reworking likely influenced the sequence. In some but not all cases, in-situ magma-sediment interaction linked to the margins of minor intrusions clearly operated Brown and Bell (2007).

A prominent hard-weathering pale grey unit (at c. 1.5 m, Figs. 2b and 3b), described as an ignimbrite by Brown (2003), and Brown and Bell (2007), occurs within the dominantly normally graded volcaniclastic layers. This unit reveals normal grading (Figs. 2b and 5) and includes a high proportion of angular alkali feldspar crystals along with subsidiary albite, sphene, zircon and quartz in a matrix dominated by pyroclastic fiamme with evidence for welding. The fiamme have devitrified to secondary minerals including quartz and clays after felsic glass with subsidiary grain boundary organic matter in places (Fig. 5). The fiamme are typically 2–5 mm long and 0.5–2 mm thick and reveal a clearly eutaxitic bedding parallel fabric which is best developed at the base of the unit and decreases along with apparent degree of welding and grain size (<1 mm) towards the top of the unit (Fig. 5a). The alkali feldspars are typically equant and c. 1 mm in diameter in the lower portion of the bed and fine up to <0.5 mm in the upper part of the bed. Clear examples of viscous pinching and moulding of fiamme around crystals is observed, and importantly is not restricted to a vertical compression axis, excluding post-emplacement compaction alone. It is from this unit that pristine magmatic zircons (Fig. 5e) were liberated for high resolution isotopic U—Pb CA-ID-TIMS dating. In one example, a zircon is observed within a fine grained crystalline felsic clast, the grain being notably fractured unlike the analysed grains (Fig. 5f). This clast appears to comprise a crystalline fragment of the associated magma plumbing system to the ignimbrite, however, it could also represent an earlier unrelated intrusion, no zircons of this character were analysed.

Above this distinct layer, the sequence comprises similar thin graded volcaniclastic beds with mixed epiclastic to pyroclastic components ranging from small granule grade up to fine grained sand with abundant organic rich mud within the matrix (Fig. 3c). At the top of the sequence a prominent layer comprising variably vesicular raggy to fluidal and elongate basaltic pyroclasts up to c. 15 cm long (Fig. 3d,e), are mixed with a dark organic rich sediment matrix. This unit forms a wedge of stratigraphy thinning from east to west across the exposure (Fig. 2). The raggy pyroclasts reveal clear evidence for plastic deformation and a fabric whereby the clasts are stretched out parallel to the well-defined bedding (Fig. 3e). Occasional dense angular blocks of finely crystalline basalt (Fig. 3e), some comprising the core to fluidal basalt bombs (Fig. 3g), occur within the bedded pyroclastic deposit along with vitreous charcoalified woody fragments. Lateral facies variations at this
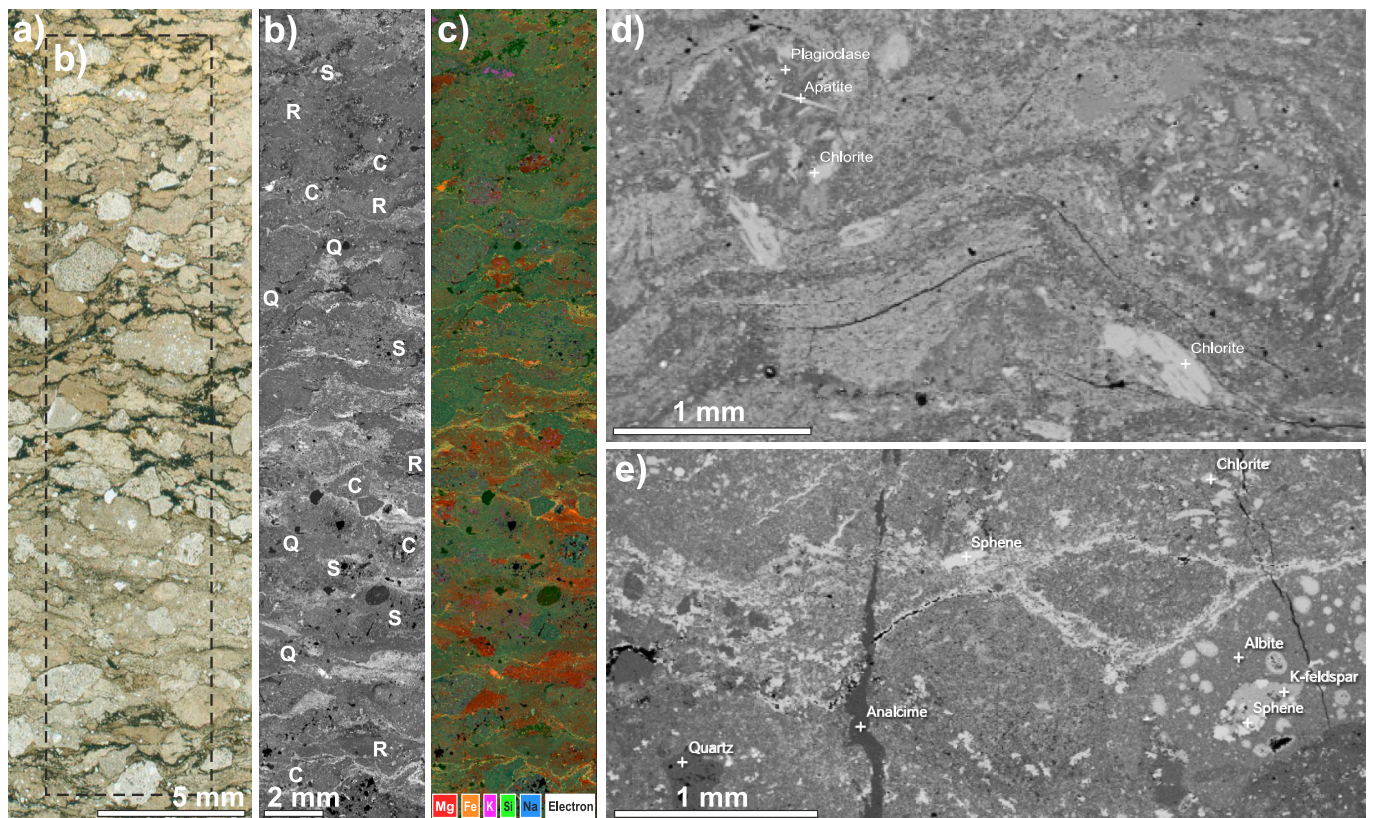
Fig. 4. a) Slide scan of volcaniclastic sediment from AIL. b) Composite SEM backscatter image (Q = quartz, C = crystalline, S = scoriaceous, R = raggy pyroclast). c) False-colour SEM backscatter image of (b) highlighting the basic Fe/Mg rich components of the deposit. d) Close up SEM image of deformed raggy pyroclasts and crystalline basalt epiclasts. e) Detail of mineralogy assemblage in SEM backscatter.
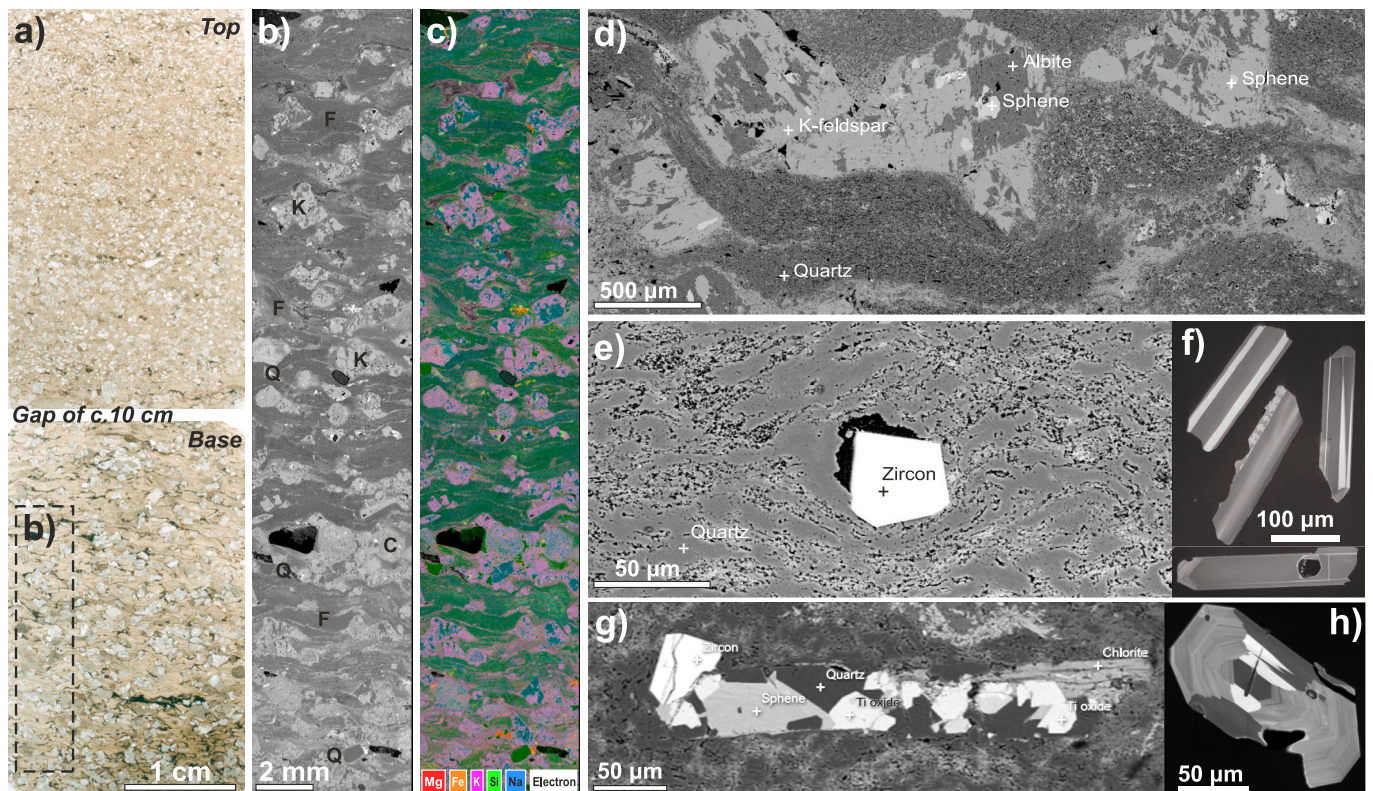
Fig. 5. a) Slide scans of the Carraig Mhór Ignimbrite. b) Composite SEM backscatter image (K=K-feldspar, Q = quartz, F = fiamme, C = crystalline). c) False-colour SEM backscatter image of (b) highlighting the dominant silicic nature of the deposit and phenocrysts of K-feldspar. d) Close up SEM image of deformed fiamme and mineral constituents. e) Pristine magmatic zircon encased in fiamme showing ductile flow textures. f) representative CL-images of zircons liberated from crushed sample interpreted to be magmatic and of the type analysed. g) Example of a single zircon in a finely crystalline felsic rock fragment. h) CL-image of a zircon from the crushed sample showing complex zoning and fractures interpreted to be a xenocryst/antecryst and not included for analysis.

level within the AIL reveal relatively well to poorly sorted and bedded volcaniclastic layers (Fig. 3f) dominantly composed of blocky angular to raggy clasts of altered basalt with less pronounced clast flattening fabrics. Clasts range from a few mm up to 20 cm diameter blocks with the same organic rich mixed sediment matrix but appear to have undergone a greater degree of quench and/or mechanical fragmentation prior to deposition than the elongate raggy pyroclasts (Fig. 3d). Local variations also include more chaotically mixed highly vesicular spatter (Fig. 3e), distributed within the sediment host.

Above this coarser grained pyroclastic wedge, friable layers of quartz dominated muddy sandstone to siltstone are present with very limited volcanic clasts occurring close to the loaded contact with the overlying L1 lava flow (Fig. 2bi). The quartz grains are often well rounded implying a mature sediment source within the catchment (e.g. potentially the Lochaline glass sand, Bailey, 1924). Fig. 3i reveals the well-bedded nature of the AIL sedimentary sequence directly beneath the L1 lava contact. The sediments are clearly loaded and deformed by the lava with localized dynamic mingling which is clearly separate from the well-bedded volcaniclastic sediment layering beneath (Fig. 3i). Many of the basaltic clasts within the graded volcaniclastic beds directly beneath the L1 lava reveal a very similar character to those found within the main overlying Carraig Mhór Bed.

Overlying the effusive Staffa Type A L1 lava flow, another thin sedimentary unit is exposed comprising organic rich dark silty volcaniclastic sandstone to fissile black muddy siltstone (Fig. 2). The exposed interbed is interpreted as stratigraphically equivalent to the upper part of the Ardtun Interbed (Jolley et al., 2024) and is at maximum 1–2 m thick. However, estimation is complicated by the intense loading and deformation caused by the overlying lava flow (Jolley et al., 2024; Williamson and Bell, 2012). The section is also intruded by thin layer-parallel pale grey (likely evolved) intrusions some of which terminate in bulbous pinch-outs within the organic rich sediments.

The Carraig Mhór Bed was described in detail by Brown and Bell (2007) who discuss several emplacement mechanisms whilst favouring an essentially in-situ peperite formation fed laterally by an invasive lava flow. The top surface of the underlying L2 lava unit is highly irregular and comprises several irregular fractured departures from the general dip surface, however, often no clear transition in vesicularity, typical of a sub-aerial lava flow top is seen. This complex upper margin likely resulted from a period of exposure and erosional scouring, stripping the weaker flow top material from the unit and leaving an irregular fractured and eroded basaltic landscape (Brown and Bell, 2007; Jolley et al., 2024). The exposure of the L2 lava is further complicated by several oblique dike intrusions that cut the cliff face. Fig. 2d presents a composite graphic facies log through the Carraig Mhór Bed which can be broadly divided into two main parts.

The lower part comprises a poorly sorted chaotic breccia of pale-green altered basaltic clasts of raggy, amoeboid, and fluidal nature, often with chilled margins, through to subsidiary internally homogenous angular basalt boulders. The unit is almost entirely matrix supported with basaltic clasts varying from boulders up to 1.5 m diameter down to coarse grained sand, all mixed with a dark organic rich sediment matrix. These basalt boulders are of almost identical geochemical composition to the overlying L3 and underlying L2 lava flows (Staffa Type C, Jolley et al., 2024). In many places, the long axis of elongate clasts reveals a bedding parallel fabric (Brown and Bell, 2007). There is no evidence for undisturbed finer grained sediments similar to those seen in the AIL at the contact between the L2 lava and the Carraig Mhór Bed, even in the relatively intricate cavities of the irregular upper surface of the L2 lava contact.

The upper sequence of the Carraig Mhór Bed comprises a similar clastic composition to below with the key difference being a distinct decrease in average clast size and increased sorting which fines upwards until it transitions into a weakly bedded volcaniclastic sequence at the top of the exposed section. The uppermost unit comprises common angular to raggy and less commonly fluidal basalt clasts very similar to those found throughout the AIL. Occasional larger clasts and blocks, distinctly above the average, along with sparse lenses of finer grained more organic rich material are observed towards the top of the sequence giving a locally weakly bedded appearance. The contact between the Carraig Mhór Bed and the overlying L3 Staffa Type C columnar basaltic lava flow is sharp and shows no evidence for dynamic interaction (Fig. 3g). A small sharp-contacted invasive lava tube is seen both in the cliff exposure (Brown and Bell, 2007) and in a more accessible prominent slumped block at the foot of the cliff where it invades into the upper CMB (Fig. 2). Brown and Bell (2007) note that the bedded upper unit is relatively undisturbed by the overlying L3 lava and, therefore, the L3 lava did not generate the CMB in-situ at this location. This inference is conformable with the observations made here, and in Jolley et al. (2024), however, we note that in Jolley et al. (2024), Brown and Bell (2007) were mistakenly referred to as invoking the L3 lava as the source of the CMB.

4.2. Age and composition of the Carraig Mhór Ignimbrite

Geochemical analyses of a sample of the Carraig Mhór Ignimbrite from within the AIL reveals a major oxide total of c. 97 wt% with 70.44 wt% SiO_2 and 9.47 wt% alkalis ($Na_2O + K_2O$) when normalized to 100% on a volatile free basis. The ignimbrite classifies as a sub-alkaline rhyolite based on the TAS (total alkalis versus SiO_2) chemical classification of Le Maitre et al. (2005), and as a rhyolite based on the Zr/Ti versus Nb/Y classification of Winchester and Floyd (1977), a classification often preferred for altered volcanic rocks due to its utilization of immobile elements. Fig. 6a presents a spider diagram of the trace elements including the rare earth elements (REE) normalized to primitive mantle (Sun and McDonough, 1989) for the rhyolite compared to two samples of lava flows from the early Mull lava pile (Hole et al., 2023; Jolley et al., 2024).

The rhyolite reveals a light REE enriched signature with clear depletions of Ti, P, Sr, Ta, and Nb. Ti and P depletion are the expected result of Fe—Ti oxide and apatite removal respectively during late-stage fractional crystallization. The rhyolite exhibits Th/Ta (10.5) and La/Ta (41.7) that are typical of Hebridean magmas that have undergone crustal contamination with Moine metasedimentary rocks, a feature it shares with Staffa lavas (Hole et al., 2015; Jolley et al., 2024; Kerr et al., 1999; Thompson et al., 1980, 1982). This is unlike the high La/Ta (up to 80) but low Th/Ta (~1.5) that characterizes Mull Plateau lavas that underwent contamination with Lewisian granulite facies metamorphic rocks (e.g. Hole et al., 2023; Jolley et al., 2024; Kerr et al., 1999). This shared contamination signature between the more basic Staffa magmas and the rhyolite analysed here suggests that the Carraig Mhór Ignimbrite likely represents a highly fractionated, crustally contaminated melt resulting from a parental magma very similar to that which fed the Staffa type basaltic magmatism, which dominates the exposed early Mull lava field (see also Hf-isotopic result below; Jolley et al., 2024).

In total nine single, euhedral, clear, colourless, high aspect ratio zircon prisms dominated by the {110} crystal face, with few and simple growth zones as imaged by CL, were selected for analyses from the Carraig Mhór Ignimbrite (Fig. 5f). Apart from a few rounded, clearly xenocrystic grains and some medium aspect ratio (1:2–1:3), yellowish and foggy grains, the separated zircons reveal a long-prismatic, euhedral morphology with pristine margins and no evidence for mechanical abrasion as may be expected for reworked detrital grains. An example of an isolated zircon enclosed within a primary fiamme texture, thought to represent pre-eruptive zircon formation from the rhyolite melt is presented in Fig. 5e. This zircon is most likely imaged down the c-axis,

hence its stubby shape. This zircon, as with the analysed long-prismatic zircons (Fig. 5f), is pristine and euhedral not displaying significant fracturing.

In one example, a zircon is identified within a felsic crystalline fragment (Fig. 5g) interpreted to represent a fragment of the magma chamber wall-rock incorporated into the pyroclastic deposit or potentially from an older intrusive unit. This zircon is euhedral but heavily fractured unlike the zircons analysed from the crushed sample. Fig. 5h reveals a similar morphology to that of Fig. 5g, displaying a large fracture and prominent fine-scaled oscillatory zoning (unlike the long-prismatic zircons), and is interpreted to possibly belong to the same zircon population as the example in Fig. 5g. This grain along with the clearly xenocrystic grains described above were not analysed as part of this study. Only zircons belonging to the long-prismatic, pristine, unfractured, simple-textured (as revealed by CL) group of grains representing the autocrystic zircons formed from the ignimbrite precursor melt were analysed in this study and so an older age for the crystalline clast in Fig. 5g cannot be excluded.

The euhedral morphology, high aspect ratios, and simple zonation with few growth zones of the analysed zircons are typical of rapid late-stage magmatic growth (Corfu et al., 2003; Cooper et al., 2014; Fig. 5). Furthermore, the presence of large, often long and thin (melt-) inclusions parallel to the c-axis, and in some cases, small-scale over-printing replacement textures (middle zircon of Fig. 5f) indicative of minor recrystallization in the presence of late-stage volatile-rich magmatic fluids (Corfu et al., 2003; Kusiak et al., 2009), supports the interpretation that the analysed, long-prismatic zircons represent latest stage pre-eruptive zircons. As such the eruption age of the deposit is interpreted to be within the weighted mean error range of the analyses. All zircon analyses are concordant and overlapping and included in the weighted mean $^{206}Pb/^{238}U$ date of 62.035 ± 0.041/0.050/0.080 Ma (2σ; MSWD = 1.84), interpreted to represent the emplacement age of the rock (Fig. 6).

The nine dated zircons were also analysed for (Lu-) Hf-isotopes. The $\varepsilon_{Hf(t)}$ of the zircons are all negative ranging between -17.60 ± 0.87 (2σ) and -19.59 ± 0.87. Apart from the analysis with the lowest and the highest $\varepsilon_{Hf(t)}$, all analyses cluster tightly and overlap (Fig. 6c) indicating that the dated zircons grew from a well-homogenised melt. Whole rock geochemistry clearly indicates that the Carraig Mhór Ignimbrite represents a fractionated, crustally contaminated melt and this is corroborated by the negative $\varepsilon_{Hf(t)}$ of the zircons. However, the fact that the Hf-isotopic signatures of the zircons are so uniform further indicates that the zircons crystallised at a late stage in the melt evolution when the crustal contaminants were well mixed in the melt, not creating an array of Hf-isotopic values reflecting the end-members of the mixed components (a fractionated "primary" melt and the crustal contaminant). Calculating depleted mantle separation model ages for the analysed zircons using a two-stage model (Griffin et al., 2002) and assuming a felsic crustal reservoir with a Lu/Hf composition of 0.05 (Bea et al., 2018) give values of c. 1.7 Ga, compatible with the Moine metasedimentary rocks being the crustal contaminant of the Carraig Mhór Ignimbrite parent melt. The Moine metasedimentary rocks are thought to dominantly comprise detritus of late Palaeoproterozoic origin (e.g., Labradorian crust; Cawood et al., 2004) averaging c. 1.7 Ga crust.

4.3. Emplacement palaeoenvironment of the Carraig Mhór Ignimbrite

Sedimentary rock samples taken for analysis of the older beds of the AIL included fine grained volcaniclastic material and bright coals. While the volcaniclastic material was barren of organic debris, the thin bright coals (<0.3 cm) were completely composed of blocky inertinite derived from drifted and possibly burnt wood. Further samples were taken from the volcaniclastic sedimentary units overlying the rhyolite up to the base of the overlying columnar jointed L1 flow. The oldest of these sedimentary rocks yielded dinoflagellate cysts. While accumulations of drifted wood are common in lacustrine depositional environments,
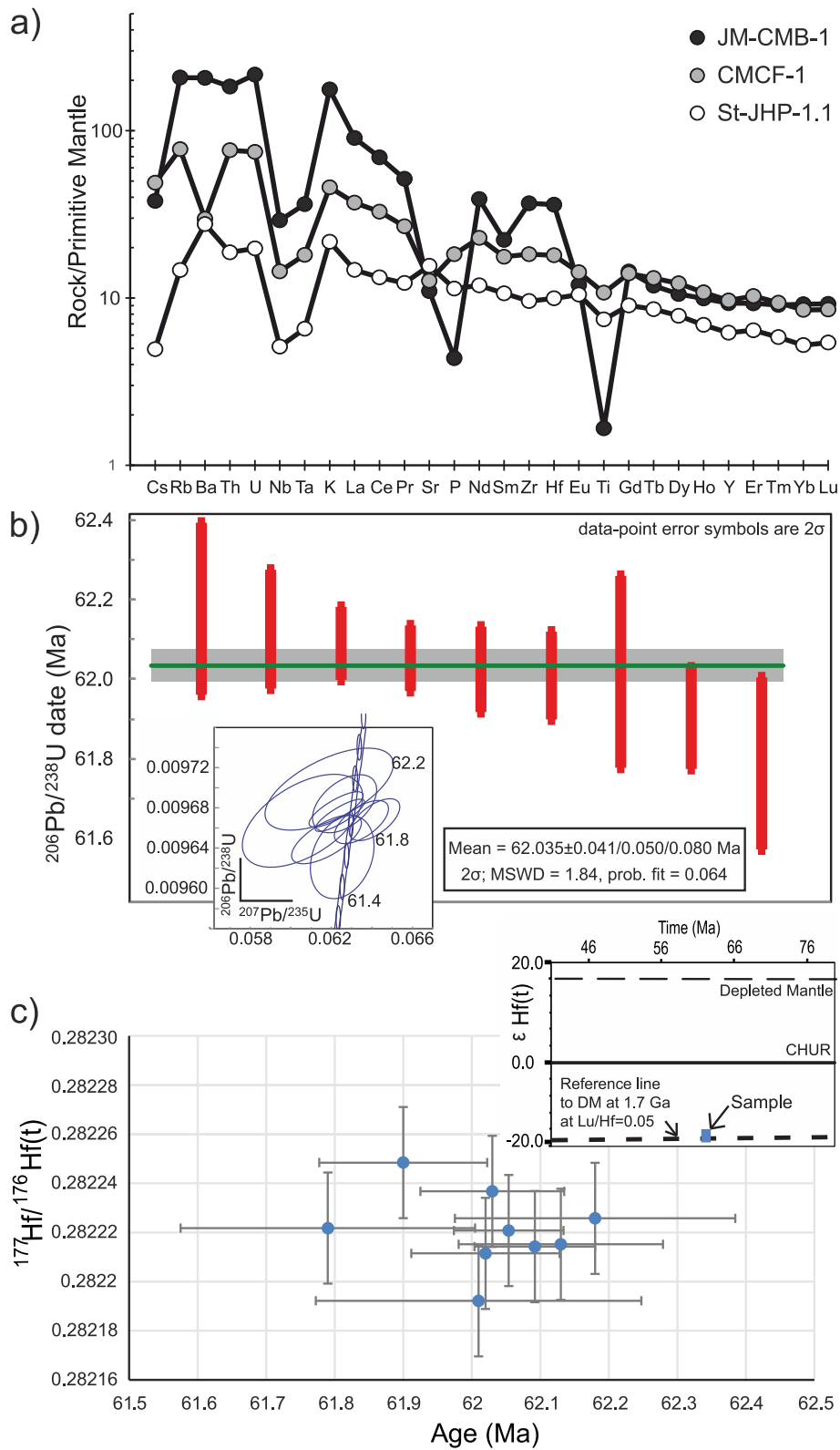
Fig. 6. a) Spider diagram showing trace elements for the Carraig Mhór Ignimbrite normalized to primitive mantle along with analyses of basaltic lava flow samples from the early Mull lava pile (Jolley et al., 2024). b) Single grain zircon $^{206}Pb/^{238}U$ dates from the Carraig Mhór Ignimbrite, with Concordia plot (lower left inset). Grey bar represents the 2σ internal error on the mean age. c) Single zircon $^{177}Hf/^{176}Hf(t)$ analyses plotted at their individual $^{206}Pb/^{238}U$ date (error bars are 2σ). Inset shows the mean $\varepsilon_{Hf(t)}$ at the interpreted emplacement age (symbol represents the mean value including 2σ error bars). The displayed reference line intersects the depleted mantle (DM) line at 1.7 Ga.

occurrences of the dinoflagellate cyst *Operculodinium* spp. indicates a brackish to saline estuarine or tidal channel water mass (D on Fig. 2e). These dinoflagellate cysts were thermally mature, reflecting the proximity of the evolved igneous sheet intruding this unit. Thermal maturation of these sediments was responsible for the poorly preserved mat of broadleaf angiosperm fossils (L on Fig. 2e), previously recorded by G. W. Lee (Bailey, 1924, p. 64). Sedimentary rocks which preserve these leaves are barren of palynomorphs, indicating a higher energy depositional environment which winnowed the silt to clay sized pollen and any microplankton. The uppermost palynology samples were taken from the top of a fining up succession underlying the L1 Staffa Type A flow (sample site marked A on Fig. 2e). These dark grey shales yielded common green algae (*Pediastrum bifidites)*.

Together, this evidence indicates that the exposed sedimentary rocks of the Ardtun Interbed equivalent at Carraig Mhór was deposited in an estuary or tidal channel. Comparable palynofloral compositions have been recorded within intra lava field tidal channels in the Hvannhagi Formation of the Faroe Islands (Jolley et al., 2022). These estuarine deposits gave way to quiescent lacustrine facies dominated by green algae within the Ardtun IB(U) sequence. High frequencies of these green algae indicate that the water mass was probably eutrophic, potentially a result of run off from contemporaneous volcanism.

5. Discussion

5.1. Volcano-sedimentary evolution of Carraig Mhór

The early phases of volcanism recorded at Carraig Mhór reveal a highly complex sequence of inter-digitated effusive, pyroclastic and epiclastic deposits. The earliest exposed stratified sedimentary deposits of the AIL were deposited in an estuarine sub-aqueous depositional environment and contain evidence for bi-modal composition pyroclastic deposits variably mixed with non-volcanic detrital quartz bearing organic rich sediments. Detailed textural examination of the ignimbrite reported by Brown (2003) reveals very minor detrital components, and clear evidence for lenticular fiamme, a eutaxitic foliation, and welding structures (Fig. 5), such as moulding against sharp crystal corners and squeezing between adjacent crystals (Gifkins et al., 2005). These features are interpreted as consistent with hot emplacement of a pyroclastic density current (PDC) forming the ignimbrite (Branney and Kokelaar, 1992), rather than mechanical compaction of altered pumice or ash alone (Gifkins et al., 2005). The reduction in both grain size and degree of welding/flattening towards the top of the layer is consistent with observations from other welded ignimbrites (Kobberger and Schmincke, 1999).

The nature of the emplacement environment suggests that the PDC was emplaced sub-aqueously and was likely fed from a sub-aerially sourced explosive rhyolitic eruption from higher up in the palaeograben system. Hot PDC's can be emplaced sub-aqueously and weld during emplacement (Kokelaar and Busby, 1992; Kokelaar and Koniger, 2000; Yamada, 1984). This process can potentially be enhanced by the suppression of volatile exsolution due to increasing pressure, resulting in lowering melt viscosity (Sparks et al., 1980), however, in the current study, based on the palynological assemblages, the water depth of emplacement was likely not significant. The chemistry of the unit is consistent with being a highly fractionated relative of the melts that produced the overlying basaltic lava flows (Jolley et al., 2024), which along with the presence of welding and an apparent lack of correlative exposures of the unit elsewhere in the region, leads to a preference for a local eruptive source rather than it being sourced from a larger distally sourced eruption.

Components similar to those within the rhyolite including altered fiamme and K-feldspar crystals occur within other layers of the AIL, but at lower abundances potentially supporting the presence of other felsic eruptions through the interval (e.g. Brown, 2003). However, these felsic components are often mixed with a greater percentage of mafic

components, and thus appear often to be locally reworked or mixed to some degree. Importantly, this demonstrates that basic magmatism was already active within the Mull area prior to the Carraig Mhór Ignimbrite eruption. This is consistent with chemical evidence for earlier basalt lava flows (Plateau D composition) sampled from the neighbouring Carsaig Bay graben system by Jolley et al. (2024), which occur stratigraphically beneath the Staffa Type A composition flows which are very similar to the L1 lava compositions in the Carraig Mhór graben.

The occurrence of graded volcaniclastic beds with mixed organic rich sediments with basaltic components including several intervals with significant proportions of raggy to fiamme-like pyroclasts showing ductile deformation, and clear examples of basalt-cored bombs, is taken as evidence for explosive basic magmatism at Carraig Mhór.

Phreatomagmatic eruptions can result from the interaction of magma with either water or unconsolidated water-saturated sediments (Wohletz et al., 2012) leading in the latter case to the intimate mixing of the two components under certain conditions (Lorenz et al., 2002; Valentine and White, 2012). Deposits from these eruptive systems can be diverse and complex, however, a distinction can be made between in-situ magma-sediment mingling leading to the formation of peperite (Skilling et al., 2002) and the explosive eruptive products resulting from these interactions that are erupted at the surface (de Herve, 2000; Lorenz et al., 2002). Eruption of mafic magma through, and explosive interaction with, the Carraig Mhór graben estuarine to lacustrine sediments, along with available surface water, is invoked as a likely source of the graded and mixed volcaniclastic deposits, similar to descriptions of phreatomagmatic deposits from Limange, France (Goër de Herve, 2000). This magmatism was likely fed by dike migration up the side of the graben bounding faults, a feature supported by abundant minor intrusions and drained feeder structures which are observed towards the east side of the Carraig Mhór study area within the AIL, Fig. 2.

The prominent wedge of elongate and plastically deformed pyroclasts near the top of the AIL clearly represents a proximal and primary, not reworked, eruption deposit and has similarities to the agglutinated spatter-like facies reported by Famelli et al. (2021) from above the first effusive lava flow at Carraig Mhór which was interpreted as related to rootless cone development. Spatter linked to littoral hydrovolcanic explosions where lavas enter the sea are reported from Hawaii (Mattox and Mangan, 1997), however, due to the presence of intimately mixed sediments, some components of either primary or rootless phreatomagmatic processes involving wet sediment incorporation appears necessary in this case. Some parts of the spatter bearing sequence resemble closely elements of deposits described as spatter bearing massive agglomerate from the Pavey Arc ignimbrite sequence (Kokelaar et al., 2007), interpreted as a spatter-bearing pyroclastic density current emplaced into a caldera lake. Other deposits described by Elliot and Hanson (2001), and Valentine and van Wyk de Vries (2014), documented as the result of phreatomagmatic eruptions from Antarctica and the Mardoux structure, France, respectively also show similarities to the elements of the studied sections. The presence of angular basalt fragments, sometimes forming the cores of vesicular bombs (Fig. 3g) also appears consistent with a phreatomagmatic explosive input into the system (e.g. Rosseel et al., 2006).

Both these lateral equivalents and the spatter-like pyroclasts were clearly erupted with some entrained organic rich sediments implying pre- to syn-emplacement mixing (Lorenz et al., 2002; Valentine and White, 2012; Valentine and Wyk de Vries, 2014). The above-described wedge of phreatomagmatic deposits could potentially form part of a small Maar-type volcano (Valentine and White, 2012), however, the limited exposure does not permit clear geometrical constraints.

The elongate and plastically deformed spatter-like clasts were clearly not destroyed by vigorous phreatomagmatic quench fragmentation which implies surface eruptions with less available water, potentially even transitioning to locally emergent conditions. This transition in the style of volcanism from locally explosive phreatomagmatism to intervals of fire-fountaining was directly followed by the first L1 lava which

signals the transition to a sub-aerial environment and effusive eruptions, albeit with clear evidence for continued lava-sediment interaction and the development of rootless cone features (Famelli et al., 2021; Jolley et al., 2024). We note here that the differentiation between rootless and intrusion fed systems is challenging with the restricted Carraig Mhór exposures, and both appear conformable with the environmental setting.

This transition reveals a gradual displacement of the drainage system as the volcanic activity progressively filled available accommodation space. Given the close association of the sequence development with magmatism, localized to potentially more regional dynamic variations in base-level, associated with local to regional magmatic plumbing/pulsing may also have contributed to relative shifts in the drainage system (e.g. Flament et al., 2013; Galland et al., 2018; Jolley et al., 2012). The volcanic hiatus associated with the Ardtun IB(U) enabled the drainage system to re-established deposition prior to effusion of the L2 Staffa Type C lava which was erupted over poorly consolidated, lacustrine sediments that were apparently not sub-aqueous at the time due to limited interaction (Jolley et al., 2024). A period of non-deposition and sub-aerial erosion which scoured and stripped away the upper surface of the L2 ponded lava is then invoked leaving a weathered and fissured surface dominantly comprising the flow core.

The Carraig Mhór Bed which directly ovelies this partly eroded surface has previously been interpreted as a graded peperite by Brown and Bell (2007) invoking a process of in-situ lava flow invasion and interaction with wet sediment accompanied by gravity settling to explain the grading. Alternative hypotheses including mass transport deposits (MTD), juvenile ballistic fall-out onto wet sediments, pyroclastic and phreatomagmatic eruptions, and PDC interaction with underlying sediments were all considered by Brown and Bell (2007) but were not preferred at the time. Clearly the CMB bed presents a texturally complex deposit with few, if any, direct equivalents described in the literature making interpretation challenging. We consider the original descriptions of the CMB by Brown and Bell (2007) detailed and comprehensive and refer the reader to their study for an eloquent discussion on the possible interpretations for the CMB.

In the current study, we find the lack of evidence for undisturbed organic rich sediments (the matrix to the CMB) at the base of the CMB, even within the intricate crevasses of the irregular upper surface of the underlying flow, hard to reconcile with an in-situ peperite-forming process. In order for the c. 10 m thick CMB to be emplaced in-situ, the thickness of pre-existing fine grained organic rich sediment would need to be several m thick and presumably have taken 100 s to 1000s of years to accumulate. Such a sediment body would be partially compacted and dewatered towards its base and would, therefore, have a sheer strength that would need to be overcome by any process promoting fluidization uniformly along the entire length of the exposed outrcrop. Peperite forming processes can certainly do this locally, however, leaving no trace of undisturbed sediments in the intricate and often narrow enclaves of the L2 flow top we feel invokes a challenging degree of uniform sediment fluidization for this setting. In particular, this process would have to be heat-driven, and as reported by Jolley et al. (2024), palynomorphs from the central and upper portion of the CMB show a low thermal alteration index implying that not all of the CMB was subjected to elevated temperatures.

The grading and fabric of the CMB is consistent along the exposed cliff face and shows no evidence for invasive lava feeders to support an in-situ emplacement model. This is again challenging, as shallow intrusions and invasive lava flows emplaced into soft sediment commonly show channelization and 'magma-finger' type flow propagation pathways with coherent magma fingers surrounded by deformed, fluidized or peperitzed sediments (Famelli et al., 2021; Galland et al., 2019; Schofield et al., 2012). At the CMB, an invasive lava would have to have propagated as a near uniform front, terminating just behind the exposure, without any portion of the coherent flow breaching the exposed cross-section. We agree with Brown and Bell (2007) that the overlying

L3 flow cannot be invoked as the feeder for in-situ peperitization, however, new chemical evidence (Jolley et al., 2024) suggests that it is essentially indistinguishable from clasts within the CMB and, therefore, may be magmatically related even if it was deposited at the exposed site afterwards.

The presence of peperite-like fluidal clasts and occurrences of local jig-saw fitting clasts (Brown and Bell, 2007) clearly invoke hot emplacement of ductile juvenile basalt clasts at least as part of the lower Carraig Mhór Bed clast populations. However, there are also large blocks of angular unchilled basalt mixed within the basal assemblage, which appear very similar in character to the underlying L2 flow core and which appear to be entrained and suspended within the deposit. With the additional observations above, these features collectively appear consistent with a stratiform mass transport deposit emplaced in two main regimes resulting in the initial lower CMB, chaotic poorly sorted deposit, followed by the more ordered and better sorted upper CMB deposit. The lower CMB is interpreted as the deposit resulting from a catastrophic dam failure further up the graben where basaltic magma interacted with a perched/dammed lacustrine sedimentary deposit including dynamic mingling eventually being breached, likely triggered by, and subsequently mixed with products from explosive phreatomagmatism similar to that invoked for intervals of the lower AIL.

This initial high-energy chaotic mass transport deposit was replaced by mixed phreatomagmatic products fed from and potentially reworked from the same eruption sequence resulting in the bedded deposits of the upper CMB. The upper CMB deposits and clast components share many similarities, but on a slightly larger scale, with the bedded volcaniclastic units from the AIL (Fig. 3), interpreted as mixed phreatomagmatic deposits. As such, we suggest a model whereby both the AIL and main CMB form a continuum of deposits linked to complex phreatomagmatic interactions between the evolving Carraig Mhór sedimentary drainage system and local magmatism. The exposures reveal intersections of these mixed deposits at differing proximities to the eruption sources ranging from primary, proximal deposits, through to more distal and increasingly reworked beds of the lower AIL. Clearly the availability and depth of water varied in association with the changing depositional environments through the exposed sequences ranging from shallow estuarine, through sub-aerial to lacustrine settings.

The gently undulating top of the CMB is not consistent with fluvial incision, and as such, this top surface may potentially represent the primary lobate surface of the deposits which are overlain by the subaerial ponded basaltic L3 lava. Given such features would not be anticipated to withstand any prolonged period of exposure without rapid erosion, it is tempting to invoke the same eruption sequence that produced the CMB, eventually transitioning to effusion and feeding the lava that penultimately overran it and preserved it, a proposition conformable with the close chemical similarity of the deposits (Jolley et al., 2024).

5.2. Age onset of the Mull lava pile

Critical to understanding NAIP magmatism in its wider context is precise and accurate absolute age dating. However, despite extensive efforts to determine the age of the NAIP by radiogenic absolute age dating methods since the 1960s, very few high precision age determinations exist for the province (Wilkinson et al., 2017). To date, the age of the igneous rocks exposed on Mull remains poorly constrained with earlier efforts to date the lava formations by $^{40}Ar/^{39}Ar$ techniques on whole rock samples yielding low precision ages. These include ages of 61.1 ± 1.2 Ma (2σ), weighted mean from Mussett (1986) recalculated in Wilkinson et al. (2017) over a range from c. 58–61 Ma, to 62.87 ± 0.48 Ma (2σ) (Chambers and Pringle, 2001), with many other analyses from this study being disregarded in the review by Wilkinson et al. (2017). Various intrusions associated with the central complex were also dated by $^{40}Ar/^{39}Ar$ in Mussett (1986) giving a weighted mean of 57.4 ± 1 Ma (Wilkinson et al., 2017), whilst an unpublished AA ID-TIMS zircon

U—Pb age of 58.5 ± 0.1 Ma by M.A. Hamilton is reported for the Loch Ba Felsite in Emeleus et al. (2005).

The age of the Mull lava pile and central complexes urgently require new high precision age determinations. The new age of 62.035 ± 0.041 Ma for the stratigraphically constrained primary pyroclastic ignimbrite described here represents to our knowledge the oldest high precision U—Pb determination from the NAIP, predating the Tardree Rhyolite by over 0.5 Myr. This age pushes the onset of bi-modal magmatism on Mull back to being one of the earliest recorded eruptive sequences of the entire province, pre-dating the Danian-Selandian boundary with implications for appraising regional magmatism and relative plate motion changes (Abdelmalak et al., 2019; Jones et al., 2017). In addition, clear evidence for pyroclastic activity within the sedimentary deposits stratigraphically below the Carraig Mhór Ignimbrite indicate that volcanism on Mull pre-dated this occurrence, and clearly merits further investigation going forward. The recent reappraisal of bio-stratigraphic and geochemical correlations across the Mull area (Jolley et al., 2024), and in the offshore basins north of the UK (Jolley et al., 2021) also support the requirement for revised assessments of the absolute and relative age relationships for this part of the province in line with the present studies results.

Finally, we note that the base of the volcano-sedimentary succession on Mull, within the deepest palaeo-graben structures, is not exposed. Occurrences of the basal contact of the lava succession are instead restricted to paleo-highs onlapped by younger lava flows. Therefore, to robustly explore the age and nature of the earliest onset of volcanism in this region, along with potentially discovering a more complete and, therefore, unique Danian marine sedimentary record in this area, scientific drilling would be required.

6. Conclusions

Within this study new evidence documenting the complex nature of early explosive volcanism on the Isle of Mull is presented along with new high precision age dating results. The following conclusions can be summarized:

1. Volcanism within the Carraig Mhór area represents some of the earliest Staffa Type magmatism exposed on the Isle of Mull and initiated with bi-modal explosive eruptions erupted into an estuarine environment.
2. Basaltic magmatism reveals evidence of phreatomagmatic eruption deposits resulting from the interaction of local feeder dikes with unconsolidated organic rich sediments which periodically transitioned to effusive eruptions as accommodation space was filled and the drainage system was displaced.
3. A prominent crystal rich rhyolitic composition ignimbrite, here termed the Carraig Mhór Ignimbrite, occurs very close to the base of the exposed succession. The ignimbrite reveals evidence for welding and is interpreted to have been emplaced sub-aqueously from a hot pyroclastic density current which deposited the stratigraphically constrained bed.
4. Pristine magmatic zircons separated from the Carraig Mhór Ignimbrite give a concordant U—Pb age of 62.035 ± 0.041 Ma revealing one of the oldest high-precision age dates for a stratigraphically constrained unit within the NAIP confirming the onset of magmatism on Mull began in the late Danian.
5. This age determination from within the estuarine sequence confirms the onshore occurrence of Danian sedimentary rocks in the UK.
6. Evidence for bedded volcaniclastic deposits below the Carraig Mhór Ignimbrite indicate that basaltic volcanism initiated on Mull earlier than this recorded age, reaching back into the Danian and clearly meriting further study.

CRediT authorship contribution statement

J.M. Millett: Writing – review & editing, Writing – original draft, Visualization, Resources, Methodology, Investigation, Formal analysis, Data curation, Conceptualization. **D.W. Jolley:** Writing – review & editing, Writing – original draft, Supervision, Resources, Methodology, Investigation, Formal analysis, Data curation, Conceptualization. **M.J. Hole:** Writing – review & editing, Writing – original draft, Validation, Supervision, Methodology, Investigation, Formal analysis, Data curation, Conceptualization. **L. Augland:** Writing – review & editing, Writing – original draft, Visualization, Software, Resources, Methodology, Investigation, Formal analysis, Data curation. **J.H. Pugsley:** Writing – review & editing, Visualization, Investigation. **G.W. McLeod:** Writing – review & editing, Validation, Investigation, Conceptualization. **S. Planke:** Writing – review & editing, Validation, Investigation.

Declaration of competing interest

The authors are not aware of any competing or conflicting interests relating to the submitted manuscript.

Appendix A. Supplementary data

Supplementary data to this article can be found online at https://doi.org/10.1016/j.lithos.2024.107729.

References

Abdelmalak, M.M., Planke, S., Polteau, S., Hartz, E.H., Faleide, J.I., Tegner, C., Jerram, D.A., Millett, J.M., Myklebust, R., 2019. Breakup volcanism and plate tectonics in the NW Atlantic. Tectonophysics 760, 267–296.

Augland, L.E., David, J., 2015. Protocrustal evolution of the Nuvvuagittuq Supracrustal Belt as determined by high precision zircon Lu–Hf and U–Pb isotope data. Earth Planet. Sci. Lett. 428, 162–171.

Augland, L.E., Andresen, A., Corfu, F., Simonsen, S.L., Andersen, T., 2012. The Beiarn nappe complex: a record of Laurentian early Silurian arc magmatism in the Uppermost Allochthon, Scandinavian Caledonides. Lithos 146, 233–252.

Bailey, E.B., 1924. Tertiary and Post-Tertiary Geology of Mull, Loch Aline, and Oban: A Description of Parts of Sheets 43, 44, 51, and 52 of the Geological Map, vol. 43. HM Stationery Office.

Baksi, A.K., Reidel, S.P., Camp, V.E., Ross, M.E., Wolff, J.A., Martin, B.S., Tolan, T.L., Wells, R.E., 2013. Timing and duration of volcanism in the Columbia river basalt group: a review of existing radiometric data and new constraints on the age of the Steens through Wanapum Basalt extrusion. In: The Columbia River Flood Basalt Province: Geological Society of America Special Paper, 497, pp. 67–85.

Ballo, E.G., Augland, L.E., Hammer, Ø., Svensen, H.H., 2019. A new age model for the Ordovician (Sandbian) K-bentonites in Oslo, Norway. Palaeogeogr. Palaeoclimatol. Palaeoecol. 520, 203–213.

Bea, F., Montero, P., Molina, J.F., Scarrow, J.H., Cambeses, A., Moreno, J.A., 2018. Lu-Hf ratios of crustal rocks and their bearing on zircon Hf isotope model ages: the effects of accessories. Chem. Geol. 484, 179–190.

Berndt, C., Planke, S., Alvarez Zarikian, C.A., Frieling, J., Jones, M.T., Millett, J.M., Brinkhuis, H., Bünz, S., Svensen, H.H., Longman, J., Scherer, R.P., et al., 2023. Shallow-water hydrothermal venting linked to the Palaeocene–Eocene thermal maximum. Nat. Geosci. 16 (9), 803–809.

Blichert-Toft, J., Albarède, F., 1997. The Lu-Hf isotope geochemistry of chondrites and the evolution of the mantle-crust system. Earth Planet. Sci. Lett. 148 (1–2), 243–258.

Bouvier, A., Vervoort, J.D., Patchett, P.J., 2008. The Lu–Hf and Sm–Nd isotopic composition of CHUR: constraints from unequilibrated chondrites and implications for the bulk composition of terrestrial planets. Earth Planet. Sci. Lett. 273 (1–2), 48–57.

Bowring, J.F., McLean, N.M., Bowring, S.A., 2011. Engineering cyber infrastructure for U-Pb geochronology: Tripoli and U-Pb_Redux. Geochem. Geophys. Geosyst. 12 (6).

Branney, M.J., Kokelaar, P., 1992. A reappraisal of ignimbrite emplacement: progressive aggradation and changes from particulate to non-particulate flow during emplacement of high-grade ignimbrite. Bulletin of Volcanology 54, 504–520.

Brown, D.J., 2003. The Nature and Origin of Breccias Associated with Central Complexes and Lava Fields of the British Tertiary Igneous Province. PhD thesis. University of Glasgow.

Brown, D.J., Bell, B.R., 2007. How do you grade peperites? J. Volcanol. Geotherm. Res. 159 (4), 409–420.

Cawood, P.A., Nemchin, A.A., Strachan, R.A., Kinny, P.D., Loewy, S., 2004. Laurentian provenance and an intracratonic tectonic setting for the Moine supergroup, Scotland, constrained by detrital zircons from the Loch Eil and Glen Urquhart successions. J. Geol. Soc. Lond. 161 (5), 861–874.

Chambers, L.M., Pringle, M.S., 2001. Age and duration of activity at the Isle of Mull Tertiary igneous centre, Scotland, and confirmation of the existence of subchrons during anomaly 26r. Earth Planet. Sci. Lett. 193 (3–4), 333–345.

Chambers, L.M., Pringle, M.S., Parrish, R.R., 2005. Rapid formation of the small Isles Tertiary centre constrained by precise 40Ar/39Ar and U–Pb ages. Lithos 79 (3–4), 367–384.

Cooper, G.F., Wilson, C.J., Charlier, B.L., Wooden, J.L., Ireland, T.R., 2014. Temporal evolution and compositional signatures of two supervolcanic systems recorded in zircons from Mangakino volcanic centre, New Zealand. Contrib. Mineral. Petrol. 167, 1–23.

Corfu, F., Hanchar, J.M., Hoskin, P.W., Kinny, P., 2003. Atlas of zircon textures. Reviews in mineralogy and geochemistry 53 (1), 469–500.

de Herve, A.G., 2000. Peperites from the Limagne trench (Auvergne, French massif central): a distinctive facies of phreatomagmatic pyroclastics. History of a semantic drift. In: *Volcaniclastic rocks, from magmas to sediments*. CRC Press, pp. 91–110.

Drake, S.M., Brown, D., Beard, A., Kumlertsakul, P., Thompson, D., Bays, C., Millar, I., Goodenough, K., 2022. Catastrophic caldera-forming eruptions and climate perturbations: the result of tectonic and magmatic controls on the Paleocene-Eocene Kilchrist Caldera, Isle of Skye, NW Scotland. Volcanica 5 (2), 397–432.

Duke, 1851. On tertiary leaf-beds in the Isle of Mull: with a note on the vegetable remains from Ardtun Head. By Prof. E. Forbes, VPGS. Quart. J. Geol. Soc. London 7 (1–2), 89–103. https://doi.org/10.1144/GSL.JGS.1851.007.01-02.22.

Eldholm, O., Grue, K., 1994. North Atlantic volcanic margins: dimensions and production rates. J. Geophys. Res. Solid Earth 99 (B2), 2955–2968.

Elliot, D.H., Hanson, R.E., 2001. Origin of widespread, exceptionally thick basaltic phreatomagmatic tuff breccia in the Middle Jurassic Prebble and Mawson Formations, Antarctica. J. Volcanol. Geotherm. Res. 111 (1–4), 183–201.

Emeleus, C.H., Bell, B.R., MacGregor, A.G., British Geological Survey, 2005. The Palaeogene Volcanic Districts of Scotland, vol. 3. British Geological Survey, Nottingham.

Famelli, N., Millett, J.M., Hole, M.J., Lima, E.F., Carmo, I.D.O., Jerram, D.A., Jolley, D. W., Pugsley, J.H., Howell, J.A., 2021. Characterizing the nature and importance of lava-sediment interactions with the aid of field outcrop analogues. J. S. Am. Earth Sci. 108, 103108.

Fisher, R.V., Schmincke, H.U., 2012. Pyroclastic Rocks. Springer Science & Business Media.

Flament, N., Gurnis, M., Müller, R.D., 2013. A review of observations and models of dynamic topography. Lithosphere 5 (2), 189–210.

Galland, O., Holohan, E., Van Wyk de Vries, B., Burchardt, S., 2018. Laboratory modelling of volcano plumbing systems: a review. In: Physical Geology of Shallow Magmatic Systems: Dykes, Sills and Laccoliths, pp. 147–214.

Galland, O., Spacapan, J.B., Rabbel, O., Mair, K., Soto, F.G., Eiken, T., Schiuma, M., Leanza, H.A., 2019. Structure, emplacement mechanism and magma-flow significance of igneous fingers–implications for sill emplacement in sedimentary basins. J. Struct. Geol. 124, 120–135.

Ganerød, M., Chew, D.M., Smethurst, M.A., Troll, V.R., Corfu, F., Meade, F., Prestvik, T., 2011. Geochronology of the Tardree rhyolite complex, Northern Ireland: implications for zircon fission track studies, the North Atlantic Igneous Province and the age of the fish Canyon sanidine standard. Chem. Geol. 286 (3–4), 222–228.

Gardner, J.S., 1887. On the leaf-beds and gravels of Ardtun, Carsaig, &c., in Mull. Quart. J. Geol. Soc. London 43 (1–4), 270–300.

Gifkins, C.C., Allen, R.L., McPhie, J., 2005. Apparent welding textures in altered pumice-rich rocks. J. Volcanol. Geotherm. Res. 142 (1–2), 29–47.

Griffin, W.L., Wang, X., Jackson, S.E., Pearson, N.J., O'Reilly, S.Y., Xu, X., Zhou, X., 2002. Zircon chemistry and magma mixing, SE China: in-situ analysis of Hf isotopes, Tonglu and Pingtan igneous complexes. Lithos 61 (3–4), 237–269.

Hamilton, M.A., Pearson, D.G., Thompson, R.N., Kelley, S.P., Emeleus, C.H., 1998. Rapid eruption of Skye lavas inferred from precise U–Pb and Ar–Ar dating of the Rum and Cuillin plutonic complexes. Nature 394 (6690), 260–263.

Hole, M.J., Natland, J.H., 2020. Magmatism in the North Atlantic Igneous Province; mantle temperatures, rifting and geodynamics. Earth Sci. Rev. 206, 102794.

Hole, M.J., Millett, J.M., Rogers, N.W., Jolley, D.W., 2015. Rifting and mafic magmatism in the Hebridean basins. J. Geol. Soc. Lond. 172 (2), 218–236.

Hole, M.J., Pugsley, J.H., Jolley, D.W., Millett, J.M., 2023. Fractional crystallization of garnet in alkali basalts at> 1.8 GPa and implications for geochemical diversity of Large Igneous Provinces. Lithos 460, 107397.

Horni, J., Hopper, J.R., Blischke, A., Geisler, W.H., Stewart, M., McDermott, K., Judge, M., Erlendsson, Ö., Árting, U., 2017. Regional distribution of volcanism within the North Atlantic Igneous Province. Geol. Soc. Lond. Spec. Publ. 447 (1), 105–125.

Huyskens, M.H., Zink, S., Amelin, Y., 2016. Evaluation of temperature-time conditions for the chemical abrasion treatment of single zircons for U–Pb geochronology. Chem. Geol. 438, 25–35.

Ickert, R.B., 2013. Algorithms for estimating uncertainties in initial radiogenic isotope ratios and model ages. Chem. Geol. 340, 131–138.

Jolley, D.W., Clarke, B., Kelley, S., 2002. Paleogene time scale miscalibration: evidence from the dating of the North Atlantic igneous province. Geology 30 (1), 7–10.

Jaffey, A.H., Flynn, K.F., Glendenin, L.E., Bentley, W.T., Essling, A.M., 1971. Precision measurement of half-lives and specific activities of U 235 and U 238. Physical review C 4 (5), 1889.

Jolley, D.W., Bell, B.R., Williamson, I.T., Prince, I., 2009. Syn-eruption vegetation dynamics, paleosurfaces and structural controls on lava field vegetation: an example from the Palaeogene Staffa Formation, Mull Lava Field, Scotland. Rev. Palaeobot. Palynol. 153 (1–2), 19–33.

Jolley, D.W., Passey, S.R., Hole, M., Millett, J., 2012. Large-scale magmatic pulses drive plant ecosystem dynamics. J. Geol. Soc. Lond. 169 (6), 703–711.

Jolley, D.W., Millett, J.M., Schofield, N., Broadley, L., 2021. Stratigraphy of volcanic rock successions of the North Atlantic rifted margin: the offshore record of the Faroe–Shetland and Rockall basins. Earth Environ. Sci. Trans. R. Soc. Edinb. 112 (2), 61–88.

Jolley, D.W., Passey, S.R., Vosgerau, H., Sørensen, E.V., 2022. Volcanic landscape controls on pre-rift to syn-rift volcano sedimentary systems: the Prestfjall Formation eruptive hiatus, Faroe Islands basalt group, Northeast Atlantic. Earth Environ. Sci. Trans. R. Soc. Edinb. 113 (2), 75–98.

Jolley, D.W., Millett, J.M., Hole, M., Pugsley, J., 2024. Integrated photogrammetry, lava geochemistry and palynological re-evaluation of the early evolution of the topographically constrained Mull Lava Field, Scotland. In: Earth and Environmental Science Transactions of the Royal Society of Edinburgh, pp. 1–25. https://doi.org/10.1017/S175569102300191. Published online 2024.

Jones, M.T., Augland, L.E., Shephard, G.E., Burgess, S.D., Eliassen, G.T., Jochmann, M. M., Friis, B., Jerram, D.A., Planke, S., Svensen, H.H., 2017. Constraining shifts in North Atlantic plate motions during the Palaeocene by U-Pb dating of Svalbard tephra layers. Sci. Rep. 7 (1), 6822.

Kelley, S., 2002. Excess argon in K–Ar and Ar–Ar geochronology. Chem. Geol. 188 (1-2), 1–22.

Kerr, A.C., Kent, R.W., Thomson, B.A., Seedhouse, J.K., Donaldson, C.H., 1999. Geochemical evolution of the Tertiary Mull volcano, western Scotland. J. Petrol. 40 (6), 873–908.

Kobberger, G., Schmincke, H.U., 1999. Deposition of rheomorphic ignimbrite D (Mogán Formation), Gran Canaria, Canary Islands, Spain. Bull. Volcanol. 60 (6), 465–485.

Kokelaar, P., Busby, C., 1992. Subaqueous explosive eruption and welding of pyroclastic deposits. Science 257 (5067), 196–201.

Kokelaar, P., Koniger, S., 2000. Marine emplacement of welded ignimbrite: the Ordovician Pitts Head Tuff, North Wales. J. Geol. Soc. Lond. 157 (3), 517–536.

Kokelaar, P., Raine, P., Branney, M.J., 2007. Incursion of a large-volume, spatter-bearing pyroclastic density current into a caldera lake: Pavey Ark ignimbrite, 70. Scafell caldera, England. Bulletin of Volcanology, pp. 23–54.

Kusiak, M.A., Dunkley, D.J., Słaby, E., Martin, H., Budzyń, B., 2009. Sensitive high-resolution ion microprobe analysis of zircon reequilibrated by late magmatic fluids in a hybridized pluton. Geology 37 (12), 1063–1066.

Le Maitre, R.W., Streckeisen, A., Zanettin, B., Le Bas, M.J., Bonin, B., Bateman, P., 2005. Igneous Rocks: A Classification and Glossary of Terms, p. 252.

Lorenz, V., Zimanowski, B., Buettner, R., 2002. On the formation of deep-seated subterranean peperite-like magma–sediment mixtures. J. Volcanol. Geotherm. Res. 114 (1–2), 107–118.

Ludwig, K.R., 2003. User's Manual for Isoplot 3.00: A Geochronological Toolkit for Microsoft Excel, vol. No. 4. Kenneth R. Ludwig.

Mattinson, J.M., 2005. Zircon U–Pb chemical abrasion ("CA-TIMS") method: combined annealing and multi-step partial dissolution analysis for improved precision and accuracy of zircon ages. Chem. Geol. 220 (1–2), 47–66.

Mattox, T.N., Mangan, M.T., 1997. Littoral hydrovolcanic explosions: a case study of lava–seawater interaction at Kilauea Volcano. J. Volcanol. Geotherm. Res. 75 (1–2), 1–17.

Millett, J.M., Hole, M.J., Jolley, D.W., Passey, S.R., Rossetti, L., 2020. Transient mantle cooling linked to regional volcanic shut-down and early rifting in the North Atlantic Igneous Province. Bull. Volcanol. 82, 1–27.

Millett, J.M., Jerram, D.A., Manton, B., Planke, S., Ablard, P., Wallis, D., Hole, M.J., Brandsen, H., Jolley, D.W., Dennehy, C., 2021. The Rosebank field, NE Atlantic: volcanic characterisation of an inter-lava hydrocarbon discovery. Basin Res. 33 (6), 2883–2913.

Mussett, A.E., 1986. 40Ar–39Ar step-heating ages of the Tertiary igneous rocks of Mull, Scotland. J. Geol. Soc. 143 (6), 887–896.

Nielsen, S.B., Stephenson, R., Thomsen, E., 2007. Dynamics of Mid-Palaeocene North Atlantic rifting linked with European intra-plate deformations. Nature 450 (7172), 1071–1074.

Patchett, P.J., Tatsumoto, M., 1981. A routine high-precision method for Lu-Hf isotope geochemistry and chronology. Contributions to Mineralogy and Petrology 75, 263–267.

Planke, S., Berndt, C., Alvarez Zarikian, C.A., 2023. Mid-Norwegian margin magmatism and paleoclimate implications. In: Proceedings of the International Ocean Discovery Program Expedition Reports, p. 396.

Rosseel, J.B., White, J.D.L., Houghton, B.F., 2006. Complex bombs of phreatomagmatic eruptions: role of agglomeration and welding in vents of the 1886 Rotomahana eruption, Tarawera, New Zealand. J. Geophys. Res. Solid Earth 111 (B12).

Saunders, A.D., Fitton, J.G., Kerr, A.C., Norry, M.J., Kent, R.W., Mahoney, J.J., Coffin, M. F., 1997. The North Atlantic igneous province. Geophys. Monogr. Am. Geophys. Union 100, 45–94.

Scherer, E., Munker, C., Mezger, K., 2001. Calibration of the lutetium-hafnium clock. Science 293 (5530), 683–687.

Schiffer, C., Doré, A.G., Foulger, G.R., Franke, D., Geoffroy, L., Gernigon, L., Holdsworth, B., Kusznir, N., Lundin, E., McCaffrey, K., Peace, A.L., 2020. Structural inheritance in the North Atlantic. Earth Sci. Rev. 206, 102975.

Schmitz, M.D., Schoene, B., 2007. Derivation of isotope ratios, errors, and error correlations for U-Pb geochronology using 205Pb-235U-(233U)-spiked isotope dilution thermal ionization mass spectrometric data. Geochem. Geophys. Geosyst. 8 (8).

Schofield, N.J., Brown, D.J., Magee, C., Stevenson, C.T., 2012. Sill morphology and comparison of brittle and non-brittle emplacement mechanisms. J. Geol. Soc. Lond. 169 (2), 127–141.

Skilling, I.P., White, J.D., McPhie, J., 2002. Peperite: a review of magma–sediment mingling. J. Volcanol. Geotherm. Res. 114 (1–2), 1–17.

Söderlund, U., Patchett, P.J., Vervoort, J.D., Isachsen, C.E., 2004. The 176Lu decay constant determined by Lu–Hf and U–Pb isotope systematics of Precambrian mafic intrusions. Earth Planet. Sci. Lett. 219 (3–4), 311–324.

Sparks, R.S.J., Sigurdsson, H., Carey, S.N., 1980. The entrance of pyroclastic flows into the sea, II. Theoretical considerations on subaqueous emplacement and welding. J. Volcanol. Geotherm. Res. 7 (1–2), 97–105.

Stoker, M.S., Holford, S.P., Hillis, R.R., 2018. A rift-to-drift record of vertical crustal motions in the Faroe–Shetland Basin, NW European margin: establishing constraints on NE Atlantic evolution. J. Geol. Soc. Lond. 175 (2), 263–274.

Storey, M., Duncan, R.A., Tegner, C., 2007. Timing and duration of volcanism in the North Atlantic Igneous Province: implications for geodynamics and links to the Iceland hotspot. Chem. Geol. 241 (3–4), 264–281.

Sun, S.-S., McDonough, W.F., 1989. Chemical and isotopic systematics of oceanic basalts: implications for mantle composition and processes. In: Saunders, A.D., Norry, M.J. (Eds.), Magmatism in the Ocean Basins, 42. Geological Society, London, Special Publications, pp. 313–345.

Svensen, H., Planke, S., Malthe-Sørenssen, A., Jamtveit, B., Myklebust, R., Rasmussen Eidem, T., Rey, S.S., 2004. Release of methane from a volcanic basin as a mechanism for initial Eocene global warming. Nature 429 (6991), 542–545.

Thompson, R.N., Gibson, I.L., Marriner, G.F., Mattey, D.P., Morrison, M.A., 1980. Trace-element evidence of multistage mantle fusion and polybaric fractional crystallization in the Palaeocene lavas of Skye, NW Scotland. J. Petrol. 21 (2), 265–293.

Thompson, R.N., Dickin, A.P., Gibson, I.L., Morrison, M.A., 1982. Elemental fingerprints of isotopic contamination of Hebridean Palaeocene mantle-derived magmas by Archaean sial. Contrib. Mineral. Petrol. 79, 159–168.

Valentine, G.A., van Wyk de Vries, B., 2014. Unconventional maar diatreme and associated intrusions in the soft sediment-hosted Mardoux structure (Gergovie, France). Bulletin of Volcanology 76, 1–16.

Valentine, G.A., White, J.D., 2012. Revised conceptual model for maar-diatremes: subsurface processes, energetics, and eruptive products. Geology 40 (12), 1111–1114.

Wilkinson, C.M., Ganerød, M., Hendriks, B.W., Eide, E.A., 2017. Compilation and appraisal of geochronological data from the North Atlantic Igneous Province (NAIP). Geol. Soc. Lond. Spec. Publ. 447 (1), 69–103.

Williamson, I.T., Bell, B.R., 2012. The Staffa Lava Formation: graben-related volcanism, associated sedimentation and landscape character during the early development of the Palaeogene Mull Lava Field, NW Scotland. Scott. J. Geol. 48 (1), 1–46.

Winchester, J.A., Floyd, P.A., 1977. Geochemical discrimination of different magma series and their differentiation products using immobile elements. Chem. Geol. 20, 325–343.

Wohletz, K., Zimanowski, B., Büttner, R., 2012. Magma–water interactions. In: Fagents, S.A., Gregg, T.K.P., Lopes, R.M.C. (Eds.), Modeling Volcanic Processes: The Physics and Mathematics of Volcanism. Published by Cambridge University Press.

Yamada, E., 1984. Subaqueous pyroclastic flows: their development and their deposits. Geol. Soc. Lond. Spec. Publ. 16 (1), 29–35.